JACS
JOURNAL OF THE AMERICAN CHEMICAL SOCIETY
Article
pubs.acs.org/JACS

Enhanced Solid-State Order and Field-Effect Hole Mobility through Control of Nanoscale Polymer Aggregation

Mark S. Chen,*[,†,§,¶] Olivia P. Lee,[†,§,¶] Jeremy R. Niskala,[†,§,¶] Alan T. Yiu,[‡,§] Christopher J. Tassone,[∥] Kristin Schmidt,[∥] Pierre M. Beaujuge,[∇] Seita S. Onishi,[†,#,§,⊥] Michael F. Toney,[∥] Alex Zettl,[#,§,⊥] and Jean M. J. Fréchet*[,†,‡,§,∇]

[†]Departments of Chemistry, [‡]Chemical and Biomolecular Engineering, and [#]Physics, University of California, Berkeley, California 94720, United States

[§]Materials Sciences Division, Lawrence Berkeley National Laboratory, Berkeley, California 94720, United States

[⊥]Kavli Energy Nanosciences Institute, University of California, Berkeley, California 94720, United States

[∥]Stanford Synchrotron Radiation Lightsource, Menlo Park, California 94025, United States

[∇] King Abdullah University of Science and Technology, Thuwal, Saudi Arabia 23955-6900

Supporting Information

ABSTRACT: Efficient charge carrier transport in organic field-effect transistors (OFETs) often requires thin films that display long-range order and close $\pi-\pi$ packing that is oriented in-plane with the substrate. Although some polymers have achieved high field-effect mobility with such solid-state properties, there are currently few general strategies for controlling the orientation of π-stacking within polymer films. In order to probe structural effects on polymer-packing alignment, furan-containing diketopyrrolopyrrole (DPP) polymers with similar optoelectronic properties were synthesized with either linear hexadecyl or branched 2-butyloctyl side chains. Differences in polymer solubility were observed and attributed to variation in side-chain shape and polymer backbone curvature. Averaged field-effect hole mobilities of the polymers range from 0.19 to 1.82 $cm^2/V{\cdot}s$, where PDPP3F-C16 is the least soluble polymer and provides the highest maximum mobility of 2.25 $cm^2/V{\cdot}s$. Analysis of the films by AFM and GIXD reveal that less soluble polymers with linear side chains exhibit larger crystalline domains, pack considerably more closely, and align with a greater preference for in-plane $\pi-\pi$ packing. Characterization of the polymer solutions prior to spin-coating shows a correlation between early onset nanoscale aggregation and the formation of films with highly oriented in-plane π-stacking. This effect is further observed when nonsolvent is added to PDPP3F-BO solutions to induce aggregation, which results in films with increased nanostructural order, in-plane $\pi-\pi$ orientation, and field-effect hole mobilities. Since nearly all π-conjugated materials may be coaxed to aggregate, this strategy for enhancing solid-state properties and OFET performance has applicability to a wide variety of organic electronic materials.

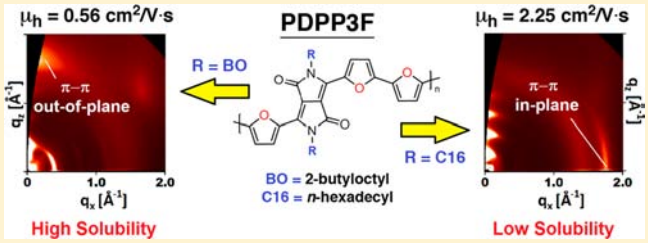

INTRODUCTION

Solution-processed organic field-effect transistors (OFETs) attract considerable research attention for their potential applications as low-cost components in large-area flexible displays,[1] radio frequency identification (RFID) tags,[2] sensors,[3] and logic circuits.[4] Through advancements in material design,[5,6] processing conditions,[7] and understanding of device physics,[8] significant progress in OFET development has led to polymer-based devices with charge mobilities that exceed 2.0 $cm^2/V{\cdot}s$.[6] In spite of these high-performing OFET polymers, it remains a challenge to correlate macromolecular structure with device performance[9] and specifically, solid-state order.[10,11]

Semiconducting films that demonstrate high field-effect mobility often consist of π-conjugated polymers with high backbone coplanarity in order to enhance effective conjugation length and charge delocalization. In the solid-state, coplanar polymer backbones promote packing with short cofacial distances[12] and highly crystalline order,[8a] thereby facilitating charge transport through a polymer film.[13] Since these polymers tend to self-assemble and aggregate, solubility is achieved by appending alkyl side chains to the backbones. Consequently, side-chain variation enables the tuning of several solid-state properties that include film morphology, crystallinity, and packing order.[14] Although these design principles provide considerable synthetic control over self-assembly and interpolymer $\pi-\pi$ distances, they fail to address how to control polymer orientation within films.

Optimal OFET performance is often achieved when the majority of $\pi-\pi$ packing aligns parallel to the substrate (in-plane), between the source and drain electrodes. Inversely, charge mobility is often diminished when cofacial packing

Received: August 27, 2013
Published: December 2, 2013

   dx.doi.org/10.1021/ja4088665 | J. Am. Chem. Soc. 2013, 135, 19229−19236

aligns perpendicular to the substrate and π-stacking is oriented out-of-plane. Most strategies for aligning conjugated polymers focus on deposition techniques and do not consider synthetic tailoring of macromolecular structure.[7a,b,15,16] The few synthetic strategies for varying $\pi-\pi$ packing orientations involve manipulation of polymer regioregularity and molecular weight.[17] By doing so, films of poly(3-hexylthiophene) have demonstrated improvements in field-effect mobility by as much as 2 orders of magnitude when films showed a preference for in-plane π-stacking. While effective for polythiophenes, these strategies are not entirely applicable to new classes of donor–acceptor polymers that often contain complex heterocyclic structures.

Diketopyrrolopyrrole (DPP)-polymers are one such class of donor–acceptor materials that have demonstrated some of the highest hole mobilities for polymer-based OFETs to date.[6a−c,18] Diketopyrrolopyrrole is a planar, bicyclic, electron-deficient chromophore that is easily accessed with various flanking moieties that include benzenes,[19] thiophenes,[20] thienothiophenes,[21] selenophenes,[22] and most recently furans (Figure 1).[23] Synthesis of furan-containing subunits is a nascent strategy

Figure 1. Synthesis of PDPP2FT and PDPP3F with linear or branched alkyl side chains via Stille cross-coupling polycondensation.

for designing new conjugated materials, despite the similarities between furan and its common sulfur-containing analog, thiophene. Oligofurans offer the potential for renewable molecular sourcing along with properties that should enhance solid-state order, like short inter-ring bond lengths and high backbone coplanarity.[24] Additionally, furan versus thiophene substitution has been shown to improve the solubility of DPP-polymers, which enables the use of less bulky solubilizing groups.[23d,e] Smaller side chains promoted closer polymer packing in blend films and substantially improved photovoltaic performance. Though not noted previously, the sizes of side chains appeared to alter the orientation of $\pi-\pi$ packing, suggesting that polymer solubility can have a significant effect on polymer alignment in the solid-state.

Herein, we thoroughly examine the effects of side-chain bulk and backbone structure on aggregation, solid-state order and OFET performance with PDPP2FT and PDPP3F. We discover that the highest performing OFET polymer, PDPP3F-C16 (up to 2.25 $cm^2/V{\cdot}s$ hole mobility), is also the least soluble material and therefore has the greatest preference for aggregation in solution. It is inferred that nanoscale solution-phase aggregates facilitate the formation of films that are optimized for OFET operation (i.e., high crystallinity, tight packing, in-plane π-stacking). These beneficial effects of aggregation are further supported by the enhancement of solid-state packing and field-effect mobility upon addition of nonsolvent to polymer solutions prior to film deposition.

RESULTS AND DISCUSSION

Polymer Synthesis and Characterization. Diketopyrrolopyrrole polymers were prepared by Stille polycondensation between a dibrominated DPP2F monomer (**1**, Figure 1) and 2,5-bis(trimethylstannyl)thiophene (**2**) or 2,5-bis-(trimethylstannyl)-furan (**3**) to furnish PDPP2FT and PDPP3F, respectively. Each polymer backbone was substituted with either linear hexadecyl (C16) or branched 2-butyloctyl (BO) side chains. Analysis by size-exclusion chromatography (SEC) reveals that the polymers have similar number average molecular weights (M_n) between 46–59 kDa and relatively narrow polydispersities (PDI) (Table 1). Both polymer backbones display considerable solubility in chloroform (>10 mg/mL), even when appended with linear hexadecyl groups. Interestingly, the analogous thiophene-containing DPP-polymers are much less soluble, thereby highlighting the profound effect of a simple atomic substitution on polymer properties.[23d,e]

In order to investigate the effects of substituting furan for thiophene on polymer geometry, density functional theory (DFT) calculations were carried out on methyl-substituted trimers of DPP3T, DPP2FT, and DPP3F using Gaussian 09 with a hybrid B3LYP correlation functional and 6-31G(d) basis set. Geometry optimized structures reveal that each trimer approaches complete planarity with very small inter-ring torsion (<4°, Figure S1 and S2). What varies the most between trimers is backbone curvature, based on the through-space distance between DPP carbonyls (Figure 2). DPP2FT shows the shortest intercarbonyl distance of 6.83 Å due to the largest bend in the conjugated backbone; DPP3F has the next shortest distance of 7.88 Å, and DPP3T exhibits the longest distance (11.25 Å). By this analysis, the conjugated backbone of DPP3T is considerably more linear than those of DPP2FT and DPP3F trimers. Notably, the backbone that displays the greatest amount of curvature among the trimers (DPP2FT) also provides the most soluble polymers (PDPP2FT, Table 1). These data support prior studies that show conjugated polymer solubility increases with greater backbone curvature.[25] Compared to linear polymers, polymers with curved backbones exhibit weaker interchain interactions, thereby diminishing aggregation and increasing solubility. Additionally, there is often a larger entropic gain for dissolution of curved polymers

Table 1. Molecular Weight Distributions, Solubilities, And Optoelectronic Properties of PDPP2FT and PDPP3F

polymer	M_n [kDa]	PDI	solubility [mg/mL]	λ_{max}^{sol} [nm][a]	λ_{max}^{film}[nm][b]	E_g[c]	HOMO[d][eV]	LUMO[d] [eV]
PDPP2FT-BO	54	1.56	28	813 (807)	808 (811)	1.41	−5.29	−3.54
PDPP2FT-C16	55	1.60	18	817 (805)	817 (820)	1.39	−5.43	−3.54
PDPP3F-BO	46	1.69	25	781 (774)	781 (788)	1.42	−5.45	−3.59
PDPP3F-C16	59	1.57	12	825 (804)	806 (807)	1.39	−5.42	−3.61

[a]Measured from chloroform solutions at 25 °C; values in parentheses were measured at the boiling point. [b]Measured from as-cast films; values in parentheses were measured after annealing at 140 °C for 30 min, followed by vacuum annealing at 110 °C (~1 mbar) for 5 days. [c]Calculated from the absorption onsets of polymer films. [d]Onsets, potentials vs Fc/Fc^+.

dx.doi.org/10.1021/ja4088665 | J. Am. Chem. Soc. 2013, 135, 19229–19236

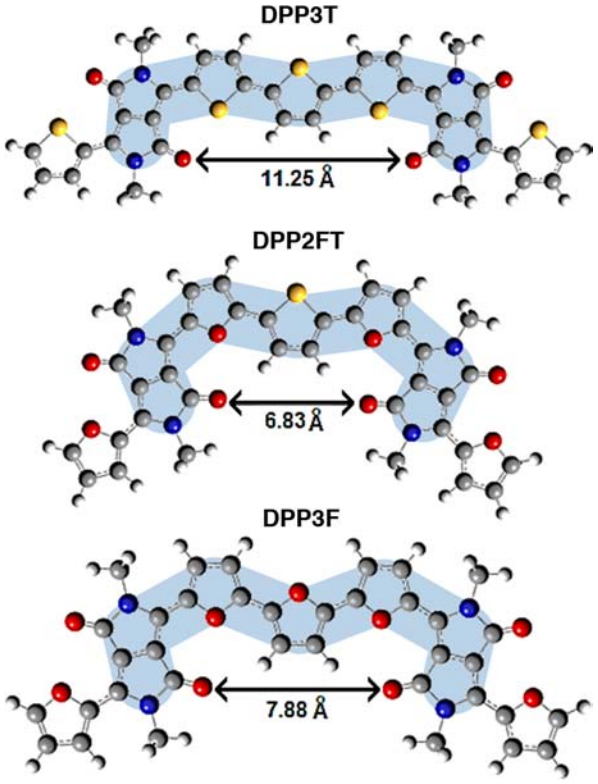

Figure 2. Geometry-optimized structures of DPP3T, DPP2FT, and DPP3F trimers obtained by DFT calculations. The extent of backbone curvature is depicted for each structure (blue highlight), along with the intercarbonyl distance between DPP subunits.

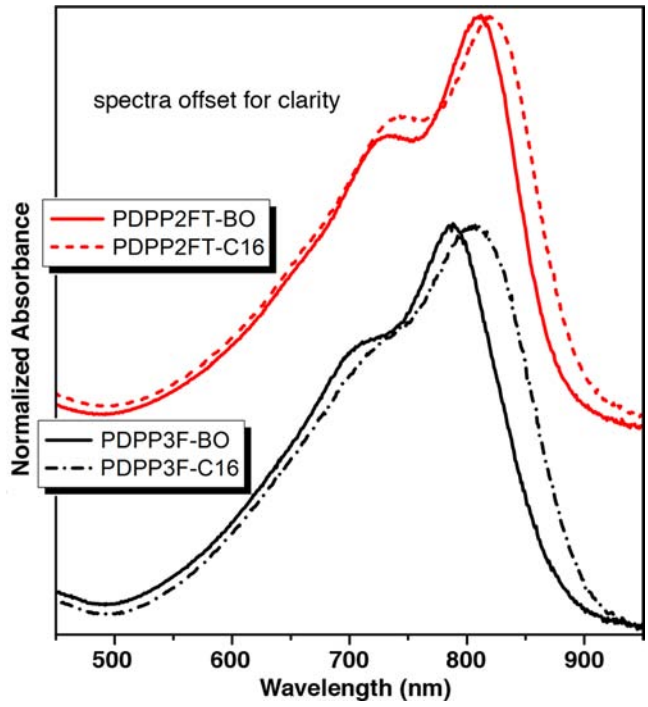

Figure 3. UV−vis−NIR absorption spectra of PDPP2FT or PDPP3F films spun from chloroform. A redshift in λ_{max} is observed for polymers substituted with linear instead of branched side chains.

as they may adopt coiled conformations that are inaccessible to more rigid, linear polymers. Therefore, the significant backbone curvature due to the furan substitution likely leads to the increased solubility of PDPP2FT when compared to PDPP3T and even PDPP3F.

Due to the similarities in molecular structure, the optoelectronic properties of each polymer appear to be comparable. Cyclic voltammetry reveals that the electrochemical energy levels are equivalent between polymers (Figure S3). UV−vis−NIR spectroscopy shows that the polymers have near identical absorption profiles, with λ_{max} values and onsets that vary only by a few nanometers (Figure 3, Table 1). From these analyses, any variation in OFET performance is likely the result of differences in film morphology rather than intrinsic polymer electronic properties.

OFET Fabrication and Performance. Hole mobility was measured from OFETs with bottom gate/top contact geometry (detailed fabrication methods are supplied in the Supporting Information, SI). Devices were fabricated by spin-coating polymer solutions from chloroform (1−3 mg/mL) onto octyltrichlorosilane (OTS)-treated SiO_2 (300 nm)/n^{2+}-Si substrates, followed by thermal deposition of Au electrodes through a shadow mask. Channel lengths and widths of 40−100 μm and 400−1600 μm, respectively, were chosen in order to minimize short channel effects. Top performing devices were thermally annealed at 140 °C for 30 min prior to top contact deposition, followed by 5 days of vacuum annealing at 110 °C (~ 1 mbar). Although differential scanning calorimetry revealed no discernible phase transitions (Figure S4), a redshift in absorption spectra of films was observed upon annealing, likely due to the removal of residual solvent and minor decreases in interpolymer spacing.

All four polymers display saturation under p-channel operation with minimal hysteresis, similar threshold voltages (V_{th}) and good hole mobility (Figure 4, Table 2).[26] PDPP2FT-C16 and PDPP2FT-BO provide hole mobilities of 0.27 and 0.19 $cm^2/V{\cdot}s$, respectively. Higher mobility (0.46 $cm^2/V{\cdot}s$) is obtained with PDPP3F-BO. The top-performing polymer in the series is PDPP3F-C16 as it demonstrates the largest I_{on}/I_{off} ratio and a maximum mobility of 2.25 $cm^2/V{\cdot}s$ (average μ_h = 1.82 $cm^2/V{\cdot}s$). Our observation that the least soluble polymer provides the highest field-effect mobility suggests that a strong tendency for PDPP3F-C16 to self-assemble contributes to the formation of well-ordered thin films.

Thin-Film Morphology. Atomic force microscopy (AFM) was employed to analyze the morphology and nanotopography of each polymer film. Films of PDPP2FT-BO and PDPP2FT-C16 show relatively small features (<50 nm) and root-mean-square roughness (R_{RMS}) values of 0.542 and 0.761 nm, respectively (Figure 5). The absence of large domains within PDPP2FT films may explain why these polymers demonstrate lower hole mobilities. In contrast, the morphology of PDPP3F films (BO and C16) show large features (≥50 nm) and patterns that suggest the presence of long-range order. Films of PDPP3F-BO show a R_{RMS} of 0.819 nm, while those of PDPP3F-C16 are the roughest (R_{RMS} = 1.233 nm). PDPP3F-C16 films even show several long, ribbon-like features that are 50 nm or more in length. These large features and increased R_{RMS} are likely the result of increased polymer crystallization and ordering during film formation. While film crystallinity is beneficial for high OFET performance, it only partially explains how PDPP3F-C16 can achieve hole mobilities >2 $cm^2/V{\cdot}s$.

Thin-Film Nanostructural Order. Grazing incidence X-ray diffraction (GIXD) was used to determine the nanostructural

dx.doi.org/10.1021/ja4088665 | J. Am. Chem. Soc. 2013, 135, 19229−19236

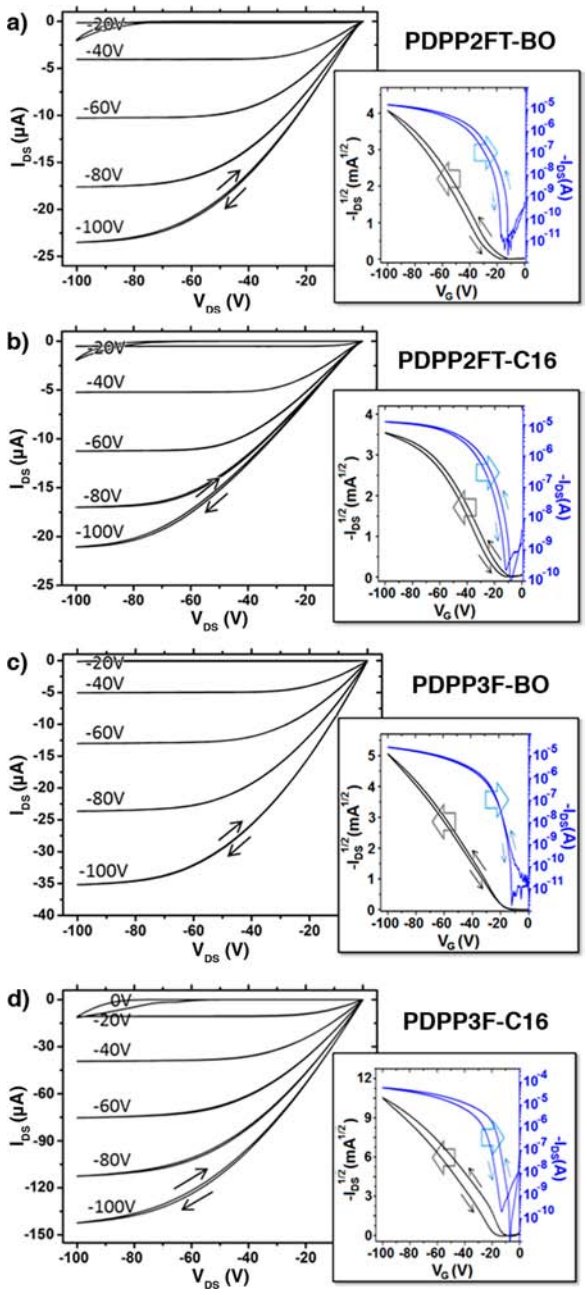

Figure 4. Output and transfer curves for OFETs fabricated with PDPP2FT and PDPP3F polymers.

Table 2. OFET Characteristics

polymer	I_{on}/I_{off}	V_{th} [V]	μ_h[a] [cm^2/V·s]
PDPP2FT-BO	10^5	−21	0.19 ± 0.08 (0.31)
PDPP2FT-C16	10^5	−12	0.27 ± 0.06 (0.35)
PDPP3F-BO	10^5	−18	0.46 ± 0.09 (0.56)
PDPP3F-C16	10^6	−11	1.82 ± 0.39 (2.25)

[a]Reported values are an average of at least 10 devices. Data in parentheses are maximum values.

order of the polymer thin films. Specifically, diffraction data enabled the measurement of cofacial $\pi-\pi$ polymer spacing, long-range crystalline order, and π-stacking orientation relative to the substrate. Small $\pi-\pi$ spacing is preferable since it reduces the energy barrier for interchain charge hopping, which is an important charge transport mechanism in polymer

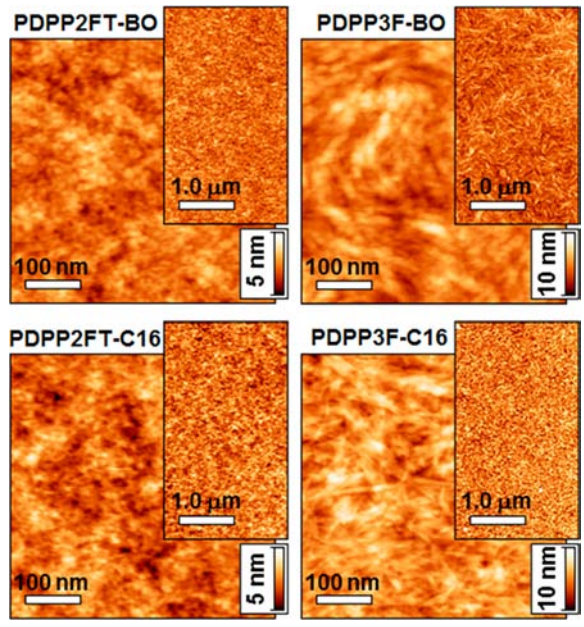

Figure 5. AFM height images of films composed of PDPP2FT and PDPP3F with BO or C16 side chains. Note the long, ribbon-like domains observable in PDPP3F-C16 films (lower right).

OFETs.[13b] The $\pi-\pi$ spacing peak is visible as a ring or partial arc at $q \sim 1.7$ Å^{-1} that corresponds to π-stacking distances of 3.82 and 3.85 Å for PDPP2FT-BO and PDPP3F-BO films, respectively (Figure 6). Films of PDPP2FT-C16 and PDPP3F-

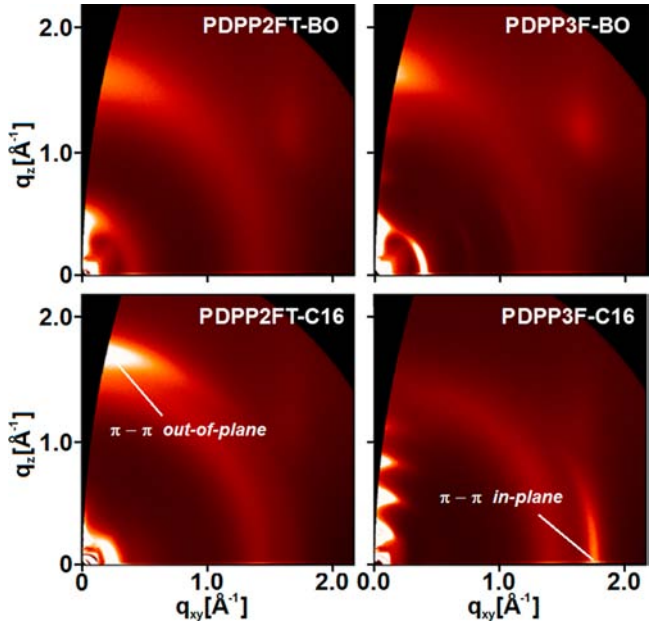

Figure 6. GIXD data from PDPP2FT and PDPP3F films. PDPP3F-C16 exhibits in-plane $\pi-\pi$ spacing, while the other three polymers pack with at least some out-of-plane $\pi-\pi$ spacing.

C16 display reduced $\pi-\pi$ spacings of 3.68 and 3.52 Å, respectively (Table 3). This side-chain effect is similar to what we observed in a previous study, where polymers substituted with linear versus branched side chains achieved tighter $\pi-\pi$ packing.[23d] The small $\pi-\pi$ spacing of C16-polymers may contribute greatly to the high hole mobilities observed in OFETs.

dx.doi.org/10.1021/ja4088665 | J. Am. Chem. Soc. 2013, 135, 19229−19236

Table 3. Thin-Film Polymer Packing Parameters Determined by GIXD

	$\pi-\pi$ spacing			lamellar spacing	
polymer	d [Å]	L_C [nm]	$R_{in/out}$	d [Å]	L_C [nm]
PDPP2FT-BO	3.82	1.1	1.49	14.68	3.1
PDPP2FT-C16	3.68	2.2	1.43	28.88	3.9
PDPP3F-BO	3.85	1.4	1.77	15.88	11.0
PDPP3F-C16	3.52	3.9	13.04	30.41	9.7

In addition to packing distances, GIXD data also provide correlation length (L_C), a measurement of the distance over which crystalline order is preserved.[9] In polymer films, a reduction in the variability of chain position and rotation corresponds to narrow peak breadth and a longer L_C. Using the full width at half-maximum (fwhm) of scattering peaks, we can determine L_C along various crystal directions via the Scherrer equation.[27] Films of PDPP2FT-BO display a $\pi-\pi$ L_C of 1.1 nm, while those of PDPP2FT-C16 show a L_C of 2.2 nm. PDPP3F-C16 films exhibit the longest L_C for $\pi-\pi$ spacing in the series (3.9 nm) that more than doubles L_C values obtained for PDPP3F-BO films (1.4 nm). It is evident from these data, that linear versus branched side chains allow polymer backbones to form crystalline nanostructures with greater order. This enhanced crystallinity of C16-polymer films, in addition to close $\pi-\pi$ spacing, enables PDPP3F-C16 films to achieve high field-effect mobilities.

Another important factor in OFET performance is the orientation of π-stacking with respect to the substrate. Films with an isotropic distribution of $\pi-\pi$ packing will display diffraction patterns with an arc of scattering intensity across all polar angles (χ). However, films with preferential orientation display anisotropic scattering intensities: in-plane $\pi-\pi$ packing leads to greater scattering intensity at low χ, along the q_{xy} axis ($q_z \sim 0$), while out-of plane packing leads to more scattering intensity along the q_z axis ($q_{xy} \sim 0$). Ratios of in-plane to out-of-plane $\pi-\pi$ scattering intensity ($R_{in/out}$) for PDPP2FT-BO and PDPP2FT-C16 films are 1.49 and 1.43, respectively, which correspond to roughly even distributions of oriented packing (see SI). Films of PDPP3F-BO show a slight preference for in-plane orientation ($R_{in/out}$ of 1.77), while PDPP3F-C16 films show that nearly all $\pi-\pi$-packing occurs in-plane with the substrate ($R_{in/out}$ = 13.04). We postulate that this dramatic enhancement in π-stacking orientation is a major factor in generating the high OFET performance of PDPP3F-C16.

Factors that Control π-Stacking Orientation. We initially hypothesized that the variation in π-stacking orientation between polymers derived from polymer–substrate interactions. Previous studies have shown that these forces can mediate molecular organization at the organic–substrate interface.[28] Nevertheless, when we alter the surface energy of the silicon substrates via functionalization with various self-assembled monolayers (i.e., octadecyltrichlorosilane, hexamethyldisilazane, trichlorosilane, perfluorooctyltrichlorosilane), the π-stacking orientation of PDPP3F remains unaffected (Figures S6 and S7). All PDPP3F-C16 films maintain a high degree of in-plane packing with $R_{in/out}$ between 11.94 and 15.87, while the films of BO-polymers still show mixed orientations of packing with $R_{in/out}$ ranging from 1.51 to 2.31. These data suggest that polymer–substrate interactions do not have a significant influence on how polymers orient relative to the substrate. If that is the case, then the alignments that we observe may be the result of interpolymer interactions that often cause polymers to aggregate in solution.

In order to investigate aggregation behavior, polymer solutions in chloroform-d were examined by nuclear magnetic resonance (NMR) spectroscopy at 40 °C. ^{1}H NMR spectra of PDPP2FT-BO show well-defined peaks for the protons at 8.54 and 6.67 ppm, which correspond to protons on the C3 and C4 positions of furan (Figure 7). Comparatively, PDPP2FT-C16

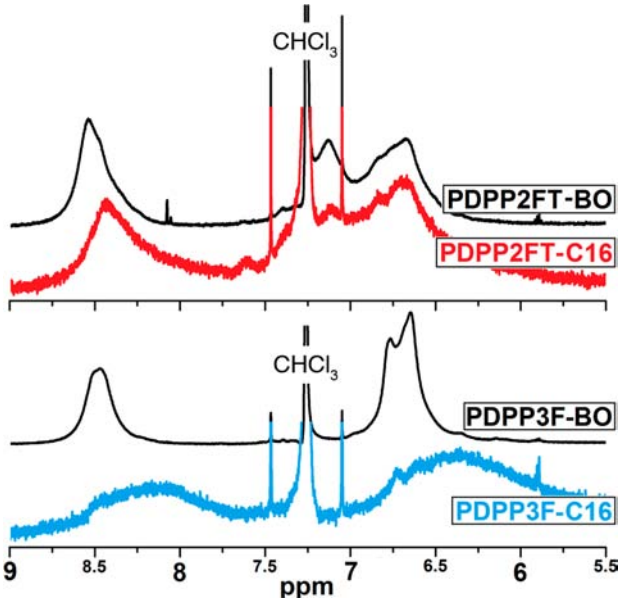

Figure 7. ^{1}H NMR spectra of PDPP2FT (top) and PDPP3F (bottom) solutions in $CDCl_3$ at 40 °C.

shows significant broadening of the aromatic peaks, alongside a minor shift upfield to 8.43 and 6.66 ppm. ^{1}H NMR spectra of PDPP3F-BO display relatively defined aromatic peaks at 8.47 and 6.64 ppm, while PDPP3F-C16 spectra show dramatic upfield peak shifts (~8.10 and ~6.36 ppm) along with extremely broad signals that are nearly indistinguishable from the baseline. The changes in ^{1}H NMR spectra upon replacing BO with C16 side chains suggest significant backbone aggregation in solution. Peak broadening can be caused by confinement effects and loss of motion averaging,[29] while upfield shifts may arise from increased π-orbital overlap and electronic shielding of protons.

Solution-phase aggregation of conjugated polymers can also be monitored by variable-temperature UV–vis–NIR absorption spectroscopy.[30] At room temperature, C16-polymers display red-shifted absorption profiles compared to BO-polymers in both film and solution. This side-chain effect is especially pronounced for PDPP3F polymers, where C16- versus BO-substitution causes the λ_{max} to redshift by 44 nm. In polymer systems, this redshift is generally attributed to increased interpolymer cofacial aggregation, which results from strong $\pi-\pi$ interactions.[31] When solutions are heated to 60 °C, the absorption profiles blueshift, corresponding to the high-temperature dissolution of polymer aggregates (Table 1, Figure S8). Spectral blueshifts are larger for C16-polymers and greatest for PDPP3F-C16 (λ_{max} blueshift = 21 nm). These absorption data reconfirm that PDPP3F-C16 is the least soluble polymer in the series and support the presence of polymer aggregates in solution.

dx.doi.org/10.1021/ja4088665 | J. Am. Chem. Soc. 2013, 135, 19229–19236

Dynamic light scattering (DLS) analysis was employed to obtain relative hydrodynamic sizes of polymer aggregates (Figure S9).[33] DLS spectra reveal that PDPP2FT-C16 aggregates have an average diameter of 69 ± 9 nm while the average size of PDPP2FT-BO aggregates is 41 ± 6 nm. Similarly, the solution aggregates of PDPP3F-C16 and PDPP3F-BO are measured to be 96 ± 21 and 24 ± 3 nm, respectively. It is evident from these results that the choice of side chains greatly affects self-assembly, where C16-polymers have a stronger tendency to form large, loosely associated aggregates in solution.

From these studies, we conclude that a polymer's lack of solubility (propensity to aggregate) correlates well with its preference for edge-on polymer packing. Conjugated polymers can aggregate and nucleate the formation of solution-phase, nanoscale regions that display short-range order.[32] The quantity and size of these assemblies depend on solubility, and generally account for only a fraction of the material in solution. During film formation these short-range ordered, π-stacked domains favor depositing parallel to the substrate in order to minimize surface free energy.[33] In turn, the crystallites direct disordered polymer chains to pack in similar fashion, resulting in the growth of larger domains that exhibit long-range order. Since less soluble polymers (i.e., C16-polymers) will form larger, ordered aggregates, their films demonstrate stronger preferences for in-plane π-stacking. Conversely, highly soluble polymers (i.e., BO-polymers) do not readily aggregate and may freely interact with the substrate, thereby allowing for kinetically favorable packing with out-of-plane π-stacking.

Effects of Nonsolvent on Morphology and Device Performance. Based on the previous discussion, we anticipate that solid-state order and field-effect mobility will be enhanced if polymer solutions are induced to aggregate. Similar strategies of promoting nanoscale polymer aggregation have been employed previously to induce crystallite formation, predetermine film morphologies,[34] and enhance the performance of organic photovoltaics[35] and OFETs.[32]

In order to promote aggregation prior to deposition, varying amounts of nonsolvent methanol (MeOH) were added to chloroform solutions of PDPP3F. Using UV−vis−NIR spectroscopy, we observe that the addition of MeOH to PDPP3F-C16 solutions (≤20%, by volume) leads to a redshift in λ_{max} (~5 nm) compared to polymer solutions in pure chloroform (Figure S10a). Although the redshift is suggestive of enhanced aggregation, the effect on device performance is minimal; films produced from these $CHCl_3$/MeOH solutions showed no improvement in crystallinity by GIXD (Figure S10b) and slightly lower average hole mobility (1.56 $cm^2/V{\cdot}s$).

In contrast, $CHCl_3$/MeOH solutions of PDPP3F-BO (≤40%, by volume) cause a λ_{max} redshift of 17 nm (Figure 8a). The resultant films exhibit increasing domain sizes and film roughness (R_{RMS}) as the amount of MeOH additive increases from 0 to 30%, by volume (Figure S11). GIXD data reveal that the $\pi-\pi$ spacing decreases from 3.85 to ~3.8 Å with the addition of MeOH to chloroform polymer solutions (Table 4, Figure S10). Additionally, increasing MeOH concentrations correlate with a greater preference for in-plane π-stacking, where films spun from 10, 20, and 30% MeOH solutions provide $R_{in/out}$ values of 1.93, 3.38, and 4.23, respectively. These PDPP3F-BO films, cast from solutions with increasing MeOH concentrations, demonstrate improved field-effect mobility, up to a maximum hole mobility of 0.77 $cm^2/V{\cdot}s$ (Figure 8b). It should be noted that solution-phase polymer aggregation has also been observed in the formation of bulk heterojunction (BHJ) films from polymer:fullerene blends containing additives like 1,8-diiodooctane and 1,8-octane-dithiol.[36] However, additive-induced aggregation promoted the formation of films with mixed, rather than in-plane, π-stacking orientations. As yet, reasons for why aggregates in those BHJ films seem to have a different effect on crystallite orientation than in our neat films remain to be determined. Nevertheless, the results of our studies explicitly demonstrate that inducing solution-phase aggregation in neat polymer solutions can improve morphology, solid-state order, and OFET performance.

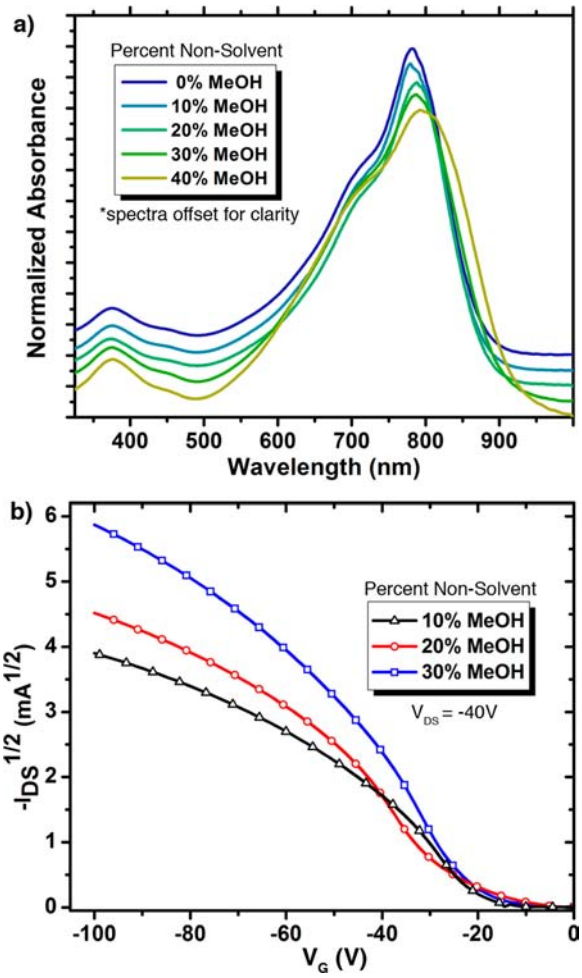

Figure 8. Effects of nonsolvent additive (MeOH) on (a) solution UV−vis−NIR absorption and (b) OFET transfer curves of PDPP3F-BO.

Table 4. GIXD and OFET Data for PDPP3F-BO Films Cast from Mixed Chloroform/Methanol Solutions

	GIXD		OFET performance		
% MeOH in solution	$\pi-\pi$ d [Å]	$R_{in/out}$	I_{on}/I_{off}	V_{th} [V]	μ_h [$cm^2/V{\cdot}s$]
10%	3.81	1.9	10^5	−20	0.40 ± 0.04 (0.45)
20%	3.78	3.4	10^6	−23	0.54 ± 0.05 (0.63)
30%	3.79	4.2	10^6	−21	0.61 ± 0.09 (0.77)

[a]Reported values are an average of at least 10 devices. Data in parentheses are maximum values.

dx.doi.org/10.1021/ja4088665 | J. Am. Chem. Soc. 2013, 135, 19229−19236

CONCLUSIONS

In this study, we examined the influence of polymer side-chain and backbone structure on solubility, morphology, and field-effect mobility using furan-containing diketopyrrolopyrrole polymers. We synthesized and characterized two polymer backbones, PDPP2FT and PDPP3F, substituted with either linear *n*-hexadecyl (C16) or branched 2-butyloctyl (BO) side chains. In OFETs, the C16-polymers out-perform their branched side chain-substituted analogs, and PDPP3F-C16 provides a maximum hole mobility of 2.25 $cm^2/V{\cdot}s$. GIXD analysis of PDPP3F-C16 films reveals that they exhibit the greatest degrees of crystallinity, closest $\pi-\pi$ spacing, and greatest preference for in-plane π-stacking alignment. Analyses of PDPP3F-C16 solutions by NMR, variable-temperature UV–vis–NIR, and DLS spectroscopies reveal that this polymer also has the strongest propensity for aggregation in solution.

We propose that solution-phase nanoscale aggregation leads to the formation of films with solid-state properties that are favorable for OFET operation. In order to support our claim, a nonsolvent additive (MeOH) was added to the PDPP3F solutions to induce polymer aggregation. While little change in nanostructural order or device performance is observed with PDPP3F-C16, PDPP3F-BO demonstrates smaller $\pi-\pi$ spacing and improved film crystallinity, π-stacking orientation, and field-effect mobility. Overall, this work elucidates fundamental structure–property relationships between polymer solubility, solid-state order, and electronic device performance.

ASSOCIATED CONTENT

Supporting Information

Experimental details, syntheses of monomers and polymers, device fabrication, and complete characterization of materials and devices. This material is available free of charge via the Internet at http://pubs.acs.org.

AUTHOR INFORMATION

Corresponding Authors

mschen@berkeley.edu
jean.frechet@kaust.edu.sa

Author Contributions

[¶]These authors contributed equally.

Notes

The authors declare no competing financial interest.

ACKNOWLEDGMENTS

This work was supported in part by the Director, Office of Science, Office of Basic Energy Sciences, Materials Science and Engineering Division, of the U.S. Department of Energy under contract no. DE-AC02-05CH11231, within the SP2-bonded Materials Program, which provided for device fabrication and electrical characterization, the Center for Advanced Molecular Photovoltaics (CAMP) under award no. KUS-C1-015-21, supported by King Abdullah University of Science and Technology (KAUST), and the Fréchet "various gifts" fund for the support of research in new materials. Portions of this research were carried out at the Stanford Synchrotron Radiation Lightsource user facility, operated on behalf of the U.S. Department of Energy, Office of Basic Energy Sciences. M.S.C. thanks the Camille and Henry Dreyfus Postdoctoral Program in Environmental Chemistry for a fellowship.

REFERENCES

(1) (a) Hamilton, R.; Heeney, M.; Anthopoulos, T.; McCulloch, I. Development of Polymer Semiconductors for Field-Effect Transistor Devices in Displays. In *Organic Electronics: Materials, Processing, Devices and Applications*. So, F., Ed.; CRC Press: Boca Raton, 2010; p 393. (b) Cicoira, F.; Santato, C. *Adv. Funct. Mater.* **2007**, *17*, 3421. (c) Gelinck, G. H.; Huitema, H. E. A.; van Veenendaal, E.; Cantatore, E.; Schrijnemakers, L.; van der Putten, J. B. P. H.; Geuns, T. C. T.; Beenhakkers, M.; Giesbers, J. B.; Huisman, B. H. *Nat. Mater.* **2004**, *3*, 106.

(2) (a) Berggren, M.; Nilsson, D.; Robinson, N. D. *Nat. Mater.* **2007**, *6*, 3. (b) Subramanian, V.; Fréchet, J. M. J.; Chang, P. C.; Lee, J. B.; Molesa, S. E.; Murphy, A. R.; Redinger, D. R.; Volkman, S. K. *Proc. IEEE* **2005**, *93*, 1330.

(3) (a) Roberts, M. E.; Sokolov, A. N.; Bao, Z. *J. Mater. Chem.* **2009**, *19*, 3351. (b) Janata, J.; Josowicz, M. *Nat. Mater.* **2003**, *2*, 19. (c) McQuade, D. T.; Pullen, A. E.; Swager, T. M. *Chem. Rev.* **2000**, *100*, 2537.

(4) (a) Fix, W.; Ullmann, A.; Ficker, J.; Clemens, W. *App. Phys. Lett.* **2002**, *81*, 1735. (b) Crone, B.; Dodabalapur, A.; Lin, Y. Y.; Filas, R. W.; Bao, Z.; LaDuca, A.; Sarpeshkar, R.; Katz, H. E.; Li, W. *Nature* **2000**, *403*, 521. (c) Drury, C.; Mutsaers, C.; Hart, C.; Matters, M.; De Leeuw, D. *App. Phys. Lett.* **1998**, *73*, 108.

(5) (a) Wang, C.; Dong, H.; Hu, W.; Liu, Y.; Zhu, D. *Chem. Rev.* **2012**, *112*, 2208. (b) Allard, S.; Forster, M.; Souharce, B.; Thiem, H.; Scherf, U. *Angew. Chem., Int. Ed.* **2008**, *47*, 4070.

(6) (a) Kang, I.; An, T. K.; Hong, J.-a.; Yun, H.-J.; Kim, R.; Chung, D. S.; Park, C. E.; Kim, Y.-H.; Kwon, S.-K. *Adv. Mater.* **2013**, *25*, 524. (b) Lee, J.; Han, A. R.; Kim, J.; Kim, Y.; Oh, J. H.; Yang, C. *J. Am. Chem. Soc.* **2012**, *134*, 20713. (c) Chen, H.; Guo, Y.; Yu, G.; Zhao, Y.; Zhang, J.; Gao, D.; Liu, H.; Liu, Y. *Adv. Mater.* **2012**, *24*, 4618. (d) Lei, T.; Dou, J. H.; Pei, J. *Adv. Mater.* **2012**, *24*, 6457. (e) Fan, J.; Yuen, J. D.; Cui, W.; Seifter, J.; Mohebbi, A. R.; Wang, M.; Zhou, H.; Heeger, A.; Wudl, F. *Adv. Mater.* **2012**, *24*, 6164. (f) Mei, J.; Kim, D. H.; Ayzner, A. L.; Toney, M. F.; Bao, Z. *J. Am. Chem. Soc.* **2011**, *133*, 20130. (g) Tsao, H. N.; Cho, D. M.; Park, I.; Hansen, M. R.; Mavrinskiy, A.; Yoon, D. Y.; Graf, R.; Pisula, W.; Spiess, H. W.; Müllen, K. *J. Am. Chem. Soc.* **2011**, *133*, 2605.

(7) (a) Wang, S.; Kiersnowski, A.; Pisula, W.; Müllen, K. *J. Am. Chem. Soc.* **2012**, *134*, 4015. (b) Wang, S.; Kappl, M.; Liebewirth, I.; Müller, M.; Kirchhoff, K.; Pisula, W.; Müllen, K. *Adv. Mater.* **2012**, *24*, 417. (c) Chua, L. L.; Zaumseil, J.; Chang, J. F.; Ou, E. C. W.; Ho, P. K. H.; Sirringhaus, H.; Friend, R. H. *Nature* **2005**, *434*, 194.

(8) (a) Rivnay, J.; Noriega, R.; Northrup, J. E.; Kline, R. J.; Toney, M. F.; Salleo, A. *Phys. Rev. B* **2011**, *83*, 121306. (b) Sirringhaus, H.; Bird, M.; Zhao, N. *Adv. Mater.* **2010**, *22*, 3893. (c) Tsao, H. N.; Cho, D.; Andreasen, J. W.; Rouhanipour, A.; Breiby, D. W.; Pisula, W.; Müllen, K. *Adv. Mater.* **2009**, *21*, 209. (d) Kline, R.; McGehee, M. *J. Macromol. Sci., Part C: Polym. Rev.* **2006**, *46*, 27.

(9) Rivnay, J.; Mannsfeld, S. C. B.; Miller, C. E.; Salleo, A.; Toney, M. F. *Chem. Rev.* **2012**, *112*, 5488.

(10) Zhang, X.; Richter, L. J.; DeLongchamp, D. M.; Kline, R. J.; Hammond, M. R.; McCulloch, I.; Heeney, M.; Ashraf, R. S.; Smith, J. N.; Anthopoulos, T. D.; Schroeder, B.; Geerts, Y. H.; Fischer, D. A.; Toney, M. F. *J. Am. Chem. Soc.* **2011**, *133*, 15073.

(11) Beaujuge, P. M.; Fréchet, J. M. J. *J. Am. Chem. Soc.* **2011**, *133*, 20009.

(12) Osaka, I.; McCullough, R. D. *Acc. Chem. Res.* **2008**, *41*, 1202.

(13) (a) Salleo, A.; Kline, R. J.; DeLongchamp, D. M.; Chabinyc, M. L. *Adv. Mater.* **2010**, *22*, 3812. (b) Coropceanu, V.; Cornil, J.; da Silva Filho, D. A.; Olivier, Y.; Silbey, R.; Brédas, J.-L. *Chem. Rev.* **2007**, *107*, 926. (c) Street, R. A.; Northrup, J. E.; Salleo, A. *Phys. Rev. B* **2005**, *71*, 165202.

(14) (a) Lee, J. S.; Son, S. K.; Song, S.; Kim, H.; Lee, D. R.; Kim, K.; Ko, M. J.; Choi, D. H.; Kim, B. S.; Cho, J. H. *Chem. Mater.* **2012**, *24*, 1316. (b) Sauvé, G.; Javier, A. E.; Zhang, R.; Liu, J.; Sydlik, S. A.; Kowalewski, T.; McCullough, R. D. *J. Mater. Chem.* **2010**, *20*, 3195. (c) Piliego, C.; Holcombe, T. W.; Douglas, J. D.; Woo, C. H.; Beaujuge, P. M.; Fréchet, J. M. J. *J. Am. Chem. Soc.* **2010**, *132*, 7595.

(d) Cho, S.; Seo, J. H.; Kim, S. H.; Song, S.; Jin, Y.; Lee, K.; Suh, H.; Heeger, A. J. *App. Phys. Lett.* **2008**, *93*, 263301.
(15) Yao, Y.; Dong, H.; Hu, W. *Polym. Chem.* **2013**, *4*, 5197.
(16) (a) Lee, J.; Han, A. R.; Hong, J.; Seo, J. H.; Oh, J. H.; Yang, C. *Adv. Funct. Mater.* **2012**, *22*, 4128. (b) Liu, Y.; Shi, Q. Q.; Dong, H. L.; Tan, J. H.; Hu, W. P.; Zhan, X. W. *Org. Electron.* **2012**, *13*, 2372. (c) Müller, C.; Aghamhammadi, M.; Himmelberger, S.; Sonar, P.; Garriga, M.; Salleo, A.; Campoy-Quiles, M. *Adv. Funct. Mater.* **2012**, *23*, 2368.
(17) Sirringhaus, H.; Brown, P.; Friend, R.; Nielsen, M.; Bechgaard, K.; Langeveld-Voss, B.; Spiering, A.; Janssen, R. A. J.; Meijer, E.; Herwig, P. *Nature* **1999**, *401*, 685.
(18) (a) Nielsen, C. B.; Turbiez, M.; McCulloch, I. *Adv. Mater.* **2013**, *25*, 1859. (b) Li, Y.; Sonar, P.; Murphy, L.; Hong, W. *Energy Environ. Sci.* **2013**, *6*, 1684.
(19) (a) Kim, C.; Liu, J.; Lin, J.; Tamayo, A. B.; Walker, B.; Wu, G.; Nguyen, T. Q. *Chem. Mater.* **2012**, *24*, 1699. (b) Chen, L.; Deng, D.; Nan, Y.; Shi, M.; Chan, P. K. L.; Chen, H. *J. Phys. Chem. C* **2011**, *115*, 11282. (c) Li, W.; Lee, T.; Oh, S. J.; Kagan, C. R. *ACS Appl. Mater. Interfaces* **2011**, *3*, 3874. (d) Wu, P. T.; Kim, F. S.; Jenekhe, S. A. *Chem. Mater.* **2011**, *23*, 4618.
(20) (a) Lin, H. W.; Lee, W. Y.; Chen, W. C. *J. Mater. Chem.* **2012**, *22*, 2120. (b) Li, Y.; Sonar, P.; Singh, S. P.; Soh, M. S.; van Meurs, M.; Tan, J. *J. Am. Chem. Soc.* **2011**, *133*, 2198. (c) Ha, J. S.; Kim, K. H.; Choi, D. H. *J. Am. Chem. Soc.* **2011**, *133*, 10364. (d) Bijleveld, J. C.; Zoombelt, A. P.; Mathijssen, S. G. J.; Wienk, M. M.; Turbiez, M.; de Leeuw, D. M.; Janssen, R. A. J. *J. Am. Chem. Soc.* **2009**, *131*, 16616. (e) Wienk, M. M.; Turbiez, M.; Gilot, J.; Janssen, R. A. J. *Adv. Mater.* **2008**, *20*, 2556.
(21) Bronstein, H.; Chen, Z.; Ashraf, R. S.; Zhang, W.; Du, J.; Durrant, J. R.; Shakya Tuladhar, P.; Song, K.; Watkins, S. E.; Geerts, Y. *J. Am. Chem. Soc.* **2011**, *133*, 3272.
(22) (a) Kronemeijer, A. J.; Gili, E.; Shahid, M.; Rivnay, J.; Salleo, A.; Heeney, M.; Sirringhaus, H. *Adv. Mater.* **2012**, *24*, 1558. (b) Shahid, M.; McCarthy-Ward, T.; Labram, J.; Rossbauer, S.; Domingo, E. B.; Watkins, S. E.; Stingelin, N.; Anthopoulos, T. D.; Heeney, M. *Chem. Sci.* **2012**, *3*, 181.
(23) (a) Sonar, P.; Singh, S. P.; Williams, E. L.; Li, Y.; Soh, M. S.; Dodabalapur, A. *J. Mater. Chem.* **2012**, *22*, 4425. (b) Sonar, P. M.; Foong, T. R. B.; Singh, S. P.; Li, Y.; Dodabalapur, A. *Chem. Commun.* **2012**, *48*, 8383. (c) Li, Y.; Sonar, P.; Singh, S. P.; Zeng, W.; Soh, M. S. *J. Mater. Chem.* **2011**, *21*, 10829. (d) Yiu, A. T.; Beaujuge, P. M.; Lee, O. P.; Woo, C. H.; Toney, M. F.; Fréchet, J. M. J. *J. Am. Chem. Soc.* **2011**, *134*, 2180. (e) Woo, C. H.; Beaujuge, P. M.; Holcombe, T. W.; Lee, O. P.; Fréchet, J. M. J. *J. Am. Chem. Soc.* **2010**, *132*, 15547.
(24) (a) Gidron, O.; Diskin-Posner, Y.; Bendikov, M. *J. Am. Chem. Soc.* **2010**, *132*, 2148−2150. (b) Bunz, U. H. F. *Angew. Chem., Int. Ed.* **2010**, *49*, 5037.
(25) Rieger, R.; Beckmann, D.; Mavrinskiy, A.; Pisula, W.; Kastler, M.; Müllen, K. *Chem. Mater.* **2010**, *22*, 5314.
(26) (a) Horowitz, G. *J. Mater. Res.* **2004**, *19*, 1946. (b) Horowitz, G. Charge Transport in Oligomers. In *Organic Field-Effect Transistors*; Bao, Z., Locklin, J., Eds.; CRC Press: Boca Raton, 2007; Vol. *128*.
(27) Roe, R. J. *Methods of X-Ray and Neutron Scattering in Polymer Science*; Oxford University Press: New York, 2000.
(28) (a) Surin, M.; Leclère, P.; De Feyter, S.; Abdel-Mottaleb, M. M. S.; De Schryver, F. C.; Henze, O.; Feast, W. J.; Lazzaroni, R. *J. Phys. Chem. B* **2006**, *110*, 7898. (b) Coffey, D. C.; Ginger, D. S. *J. Am. Chem. Soc.* **2005**, *127*, 4564.
(29) (a) Brown, S. P.; Spiess, H. W. *Chem. Rev.* **2001**, *101*, 4125. (b) Collison, C. J.; Rothberg, L. J.; Treemaneekarn, V.; Li, Y. *Macromolecules* **2001**, *34*, 2346.
(30) (a) Amrutha, S.; Jayakannan, M. *J. Phys. Chem. B* **2008**, *112*, 1119. (b) Nguyen, T.-Q.; Doan, V.; Schwartz, B. J. *J. Chem. Phys.* **1999**, *110*, 4068.
(31) (a) Koeckelberghs, G.; De Cremer, L.; Persoons, A.; Verbiest, T. *Macromolecules* **2007**, *40*, 4173. (b) Li, Y.; Vamvounis, G.; Holdcroft, S. *Macromolecules* **2002**, *35*, 6900. (c) Xu, B.; Holdcroft, S. *Macromolecules* **1993**, *26*, 4457.
(32) (a) Steyrleuthner, R.; Schubert, M.; Howard, I.; Klaumünzer, B.; Schilling, K.; Chen, Z.; Saalfrank, P.; Laquai, F.; Facchetti, A.; Neher, D. *J. Am. Chem. Soc.* **2012**, *134*, 18303. (b) Nguyen, T.-Q.; Doan, V.; Schwartz, B. J. *J. Chem. Phys.* **1999**, *110*, 4068.
(33) Zhao, L. H.; Png, R.-Q.; Zhuo, J.-M.; Wong, L.-Y.; Tang, J.-C.; Su, Y.-S.; Chua, L.-L. *Macromolecules* **2011**, *44*, 9692.
(34) Millstone, J. E.; Kavulak, D. F. J.; Woo, C. H.; Holcombe, T. W.; Westling, E. J.; Briseno, A. L.; Toney, M. F.; Fréchet, J. M. J. *Langmuir* **2010**, *26*, 13056.
(35) (a) Qian, D.; Ye, L.; Zhang, M.; Liang, Y.; Li, L.; Huang, Y.; Guo, X.; Zhang, S.; Tan, Z. a.; Hou, J. *Macromolecules* **2012**, *45*, 9611. (b) Moule, A. J.; Allard, S.; Kronenberg, N. M.; Tsami, A.; Scherf, U.; Meerholz, K. *J. Phys. Chem. C* **2008**, *112*, 12583. (c) Moulé, A. J.; Meerholz, K. *Adv. Mater.* **2008**, *20*, 240.
(36) (a) Kim, D. H.; Ayzner, A. L.; Appleton, A. L.; Schmidt, K.; Mei, J.; Toney, M. F.; Bao, Z. *Chem. Mater.* **2013**, *25*, 431. (b) Rogers, J. T.; Schmidt, K.; Toney, M. F.; Kramer, E. J.; Bazan, G. C. *Adv. Mater.* **2011**, *23*, 2284.